Olefin Chemistry in a Premixed *n*-Heptane Flame

Hongzhi R. Zhang,* Eric G. Eddings, and Adel F. Sarofim

Department of Chemical Engineering, University of Utah, Salt Lake City, Utah 84112

Received May 1, 2006. Revised Manuscript Received December 3, 2006

Three different *n*-heptane mechanisms were used to simulate a fuel-rich normal heptane premixed flame in order to identify major reaction pathways for olefin formation and consumption and areas of uncertainties of these reactions. Olefins are formed mainly via β-scission and hydrogen abstraction, and smaller olefins are sometimes formed by combination of allylic radicals and H/CH_3 radicals. Olefins are consumed by direct decomposition, radical-addition, and hydrogen-abstraction reactions. Isomerization between alkyl radicals plays an important role in olefin formation and in determining olefin species distribution. Peroxy radicals contribute to the olefin formation in the low-temperature region, but further studies are needed to resolve many uncertainties. Simulation results using the Pitsch, LLNL, and Utah heptane mechanisms were compared to experimental concentration profiles of selected species, and the uncertainties in the olefin chemistry thus identified are discussed. The discrepancies in the computed concentrations of most olefin species are usually due to the combined effects of uncertainties in the kinetics of β-scission and isomerization reactions. Resolving these uncertainties in *n*-heptane combustion chemistry is critical for building practical mechanisms for the larger paraffins that are major components of liquid aviation and diesel transportation fuels. In addition, olefin chemistry is critical to any combustion mechanisms that focus on the soot formation, because products of olefin decomposition such as C_3H_x and C_4H_x species are well-known precursors for the formation of the first aromatic ring.

Introduction

A complete understanding of carbon flow through the major reaction pathways of normal alkane combustion is one of the major foci of the combustion community because normal paraffins are found to be major components in liquid transportation fuels. The experimental and modeling studies of *n*-heptane combustion are abundant in the literature[1−5] as a result of the acceptance of *n*-heptane as the indicator fuel for gasoline octane rating and as a popular surrogate component for diesel and kerosene fuels.

Experimental and Numerical Studies of Normal Heptane. Olefin is one important class of species in premixed flames, and concentration profiles of olefins are often measured in experiments. For example, Ingemarsson and co-workers[6] measured the concentration profiles of six 1-alkene species (C_2−C_7) in their *n*-heptane oxidation experiment of a premixed laminar flame, and El Bakali et al.[2] reported concentration profiles of 1-alkenes in a rich laminar premixed *n*-heptane/O_2/N_2 flame ($\Phi = 1.9$). The same Orleans group also studied four low-pressure premixed flames[7] with a wide spectrum of equivalence ratios from lean ($\Phi = 0.7$) to rich ($\Phi = 2.0$). Later they extended the normal heptane combustion experiments to atmospheric pressure in a similar study with equivalence ratios at 1.0, 1.5,[8] and 1.9.[3] Gas chromatography was used to identify structural isomers, even to distinguish the cis and trans configurations of olefins that could not be distinguished in earlier experiments using mass spectrometry,[2] and to provide added insights in how olefins are formed and consumed.

Normal heptane mechanisms have been proposed by Held,[5] Pitsch,[9] Vovelle,[10] Ranzi,[11] Pitz,[4] and their co-workers, validated with experimental data of counter-flow diffusion flames, premixed flames, ignition behind reflected shock waves, combustion in rapid compression machines, continuously stirred reactors and high-pressure turbulent flow reactors. Also abundantly found in the literature are comparisons of the numerical performance of different mechanisms, tested with experimental data in laminar flame speed,[12] ignition delay,[13] and the OH concentration time histories[14] at reflected shock waves.

Earlier Studies of Olefin Chemistry. An extensive literature of olefin formation and consumption chemistry, not necessary with heptane fuel, complements the publications on experiments and forms an important part of the combustion modeling effort. Carriere and co-workers[15] modeled ethylene combustion in a flow reactor and in a low-pressure, premixed laminar flame. A

* Corresponding author. E-mail: westshanghai@yahoo.com.

(1) Simmie, J. M. *Prog. Energy Combust. Sci.* **2003**, *29* (6), 599.
(2) El Bakali, A.; Delfau, J. L.; Vovelle, C. *Combust. Sci. Technol.* **1998**, *140*, 69.
(3) El Bakali, A.; Delfau, J. L.; Vovelle, C. *Combust. Flame* **1999**, *118*, 381.
(4) Seiser, R.; Pitsch, H.; Seshadri, K.; Pitz, W. J.; Curran, H. J. *Proc. Combust. Inst.* **2000**, *28*, 2029.
(5) Held, T. J.; Marchese, A. J.; Dryer, F. L. *Combust. Sci. Technol.* **1997**, *123*, 107.
(6) Ingemarsson, A. T.; Pedersen, J. R.; Olsson, J. O. *J. Phys. Chem. A* **1999**, *103* (41), 8222.
(7) Doute, C.; Delfau, J. L.; Akrich, R.; Vovelle, C. *Combust. Sci. Technol.* **1997**, *124*, 249.
(8) Vovelle, C. Personal communication, 2001.
(9) Pitsch, H. Personal communication, 2001.
(10) Doute, C.; Delfau, J. L.; Vovelle, C. *Combust. Sci. Technol.* **1999**, *147*, 61.
(11) Ranzi, E.; Gaffuri, P.; Faravelli, T.; Dagaut, P. *Combust. Flame* **1995**, *103*, 91.
(12) Davis, S. G.; Law, C. K. *Proc. Combust. Inst.* **1998**, *27*, 521.
(13) Davidson, D. F.; Horning, D. C.; Hanson, R. K.; Hitch, B. 22nd International Symposium on Shock Waves, London, July 18−23,1999; paper 360.
(14) Davidson, D. F.; Herbon, I. T.; Horning, D. C.; Hanson, R. K. *Int. J. Chem. Kinet.* **2001**, *33* (12), 775.
(15) Carriere, T.; Westmoreland, P. R.; Kazakov, A.; Stein, Y. S.; Dryer, F. L. *Proc. Combust. Inst.* **2002**, *29*, 1257.

10.1021/ef060195h CCC: $37.00
Published on Web 01/13/2007

propylene model with 262 species and 1295 reactions from automatic mechanism generation was tested with ignition delay time in a shock tube[16] and with experimental data obtained in a jet-stirred reactor.[17] Heyberger et al.[16] validated a mechanism of butene with 377 reactions and 180 species with experimental data from a jet-stirred reactor.

Importance of Olefin Chemistry in Numerical Combustion. The olefin chemistry is critical in modeling of many commercial fuels such as gasoline, because olefins are fuel fractions from thermocracking process. Olefins are also very important combustion products, especially for validating the fuel consumption rate in the combustion of paraffins, because they are always produced earlier in combustion, via hydrogen abstraction and β-scission, than alkynes, paraffins, dienes, and other intermediates. Olefins also play an important role for the formation of aromatics in the combustion system. For example, the dominant formation routes of benzene or phenyl radical usually involve following reactions

$$2\ \text{propargyl radical} = \text{benzene/(phenyl radical} + \text{H)}$$

$$C_4H_x\ \text{species} + C_2H_2 = \text{(phenyl radical/benzene)} + \text{H}$$

$$\text{fulvene} + \text{H} = \text{benzene} + \text{H}$$

The precursors of aromatic compounds are formed directly from or indirectly bridged by olefin species. For example, the intermediate fulvene is formed mainly via the combination of propargyl (H_2CCCH) and allyl radicals (H_2CCHCH_2); propargyl radical comes from the decomposition of 1,2-butadiene ($CH_2{=}C{=}CH{-}CH_3 \rightarrow H_2CCCH$) and allyl radical ($H_2CCHCH_2 \rightarrow H_2CCCH_2 \rightarrow H_2CCCH$); allyl radical is formed exclusively from the thermal decomposition of larger olefins or from the hydrogen abstraction of propylene. The 1,2- and 1,3- butadienes are the principal sources of C_4H_5 isomers. These dienes come from butene isomers via intermediates of butenyl radicals C_4H_7 ($CH_2{=}CH{-}CH^{\bullet}{-}CH_3$ or $CH_2{=}CH{-}CH_2{-}CH_2^{\bullet}$). C_2H_2 is formed from dehydrogenation of C_2H_4 ($CH_2{=}CH_2 \rightarrow C_2H{=}CH^{\bullet} \rightarrow CH{\equiv}CH$).

Uncertainties in the olefin chemistry have a significant impact on the formation rate of benzene and other aromatics that are identified as one class of notable pollutants and carcinogens released from combustion systems, in addition to being soot precursors. In summary, the evolution of olefins provides vital information for understanding the combustion phenomena of large hydrocarbon fuels, especially for the rate of fuel consumption and aromatic formation.

In the current study, major reaction pathways of olefin species will be mapped out by comparing reaction rates of competing routes that are calculated from simulation results for a premixed flame. The relative importance of each reaction pathway and the impact of its kinetic uncertainty on numerical results will be discussed. In addition, the impact of the omission/inclusion, for purposes of reducing the size of the kinetic model, of the low-temperature chemistry on the kinetics at higher temperatures will also be reported. Conclusions from the current study should provide a solid base for future mechanism generation, in which rates of known reactions will be improved, and new pathways may be discovered in light of resulting deviations that suggest missing channels.

(16) Heyberger, B.; Belmekki, N.; Conraud, V.; Glaude, P. A.; Fournet, R.; Battin-Leclerc, F. *International Journal of Kinetics* **2002**, *34*, 666.

(17) Heyberger, B.; Battin-Leclerc, F.; Warth, V.; Fournet, R.; Come, G. M.; Scacchi, G. *Combust. Flame* **2001**, *126*, 1780.

Experimental Data and Numerical Models

The specifications of the Pitsch,[9] Utah, and LLNL reduced[4] normal heptane mechanisms used in this study, as well as their requirements of computing resources, have been discussed elsewhere.[18]

The experimental data of a fuel-rich laminar premixed *n*-heptane flame at atmospheric pressure with an equivalence ratio of 1.9[3] were reexamined in this study using the three mechanisms in order to identify major reaction pathways of olefin formation and consumption. The simulator used for this study was CHEMKIN III,[19] and the thermodynamics data of species were obtained from the CHEMKIN thermodynamic database[20] or estimated by THERGAS[21] employing Benson's additivity theory.[22] The transport properties of species were obtained from the CHEMKIN transport database[23] or estimated from the transport properties of similar species.

Cross-Mechanism Reaction Pathway Analysis

***β*-Scission.** Hydrogen abstraction was identified to be the major fuel-consumption pathway,[18] although it is surpassed by thermal decomposition at high temperatures (above 1400−1500 K). Despite the differences in chemical nature and reaction rate, both thermal decomposition and hydrogen-abstraction reactions yield a same class of product, alkyl radicals. Alkyl radicals convert to each other, and isomerization may significantly shift the olefin distribution. Almost all alkyl radicals decompose via β-scission into one smaller alkyl radical and one olefin, usually by breaking a C−C δ bond. Cascading alkyl radical decomposition (with alkyl radical isomerization) combined with olefin chemistry is adequate in describing the whole fuel-consumption process if appropriate kinetic parameters are available to these reactions. In some β-scission reactions, one hydrogen radical is produced instead of a smaller alkyl radical; however, these reactions are extremely unfavorable, because 40−55 kJ/mol more is needed to break a C−H bond than a C−C bond at 25 °C.[24]

There are at most two possible β-scission reactions for each alkyl radical isomer via a rupture of a C−C bond, as shown by the following list of major β-scission reactions for *n*-heptyl radicals. Arrhenius parameters for these reactions are provided in Table 1, in addition to comparisons of rates that are calculated at 1200 K for these reactions.

(18) Zhang, H. R.; Eddings, E. G.; Sarofim, A. F. An evaluation of the fuel consumption pathways for normal heptane in premixed and opposed diffusion flames. *Energy Fuels* **2007**, submitted.

(19) Kee, R. J.; Rupley, F. M.; Miller, J. A.; Coltrin, M. E.; Grcar, J. F.; Meeks, E.; Moffat, H. K.; Lutz, A. E.; Dixon-Lewis, G.; Smooke, M. D.; Warnatz, J.; Evans, G. H.; Larson, R. S.; Mitchell, R. E.; Petzold, L. R.; Reynolds, W. C.; Caracotsios, M.; Stewart, W. E.; Glarborg, P.; Wang, C.; Adigun, O.; Houf, W. G.; Chou, C. P.; Miller, S. F. *Chemkin Collection*, release 3.7.1; Reaction Design, Inc.: San Diego, CA, **2003**.

(20) Kee, R. J.; Rupley, F. M.; Miller, J. A. *The Chemikin Thermodynamic Data Base*; Technical Report SAND87-8215; Sandia National Laboratories: Albuquerque, NM, 1987.

(21) Muller, C.; Michel, V.; Scacchi, G.; Côme, G. M. *J. Chim. Phys.* **1995**, *92*, 1154.

(22) Benson, S. W.; Cruickshank, F. R.; Golden, D. M.; Haugen, G. R.; O'Neal, H. E.; Rodgers, A. S.; Shaw, R.; Walsh, R. *Chem. Rev.* **1969**, *69*, 279.

(23) Kee, R. J.; Dixon-Lewis, G.; Warnatz, J.; Coltrin, M. E.; Miller, J. A. *A Fortran Computer Package for the Evaluation of Gas-Phase, Multicomponent Transport Properties*; Technical Report SAND86-8246; Sandia National Laboratories: Albuquerque, NM, 1986.

(24) Kerr, J. A.; Stocker, D. W. In *CRC Handbook of Chemistry and Physics*; Lide, D. R., Ed.; CRC Press: Boca Raton, FL, 2000−2001; Vol. 81, pp 9/64−9/67.

$$CH_3CH_2CH_2CH_2CH_2CH_2CH_2^{\bullet} \rightarrow C_2H_4 + CH_3CH_2CH_2CH_2CH_2^{\bullet} \quad (1)$$

$$CH_3CH_2CH_2CH_2CH_2CH{\cdot}CH_3 \rightarrow CH_3CH_2CH_2CH_2CH_2CH{=}CH_2 + H \quad (2)$$

$$CH_3CH_2CH_2CH_2CH_2CH{\cdot}CH_3 \rightarrow CH_2{=}CHCH_3 + CH_3CH_2CH_2CH_2^{\bullet} \quad (3)$$

$$CH_3CH_2CH_2CH_2CH{\cdot}CH_2CH_3 \rightarrow CH_2{=}CHCH_2CH_3 + CH_3CH_2CH_2^{\bullet} \quad (4)$$

$$CH_3CH_2CH_2CH_2CH{\cdot}CH_2CH_3 \rightarrow CH_3CH_2CH_2CH_2CH{=}CH_2 + CH_3^{\bullet} \quad (5)$$

$$CH_3CH_2CH_2CH{\cdot}CH_2CH_2CH_3 \rightarrow CH_3CH_2CH_2CH{=}CH_2 + CH_3CH_2^{\bullet} \quad (6)$$

The primary heptyl radical is formed at a much slower rate than those of its secondary isomers except at very high temperatures because of the stronger primary C−H bond.[18] Thus, as shown in Figure 1, the rate of reaction 1 is the second slowest for all three mechanisms. Similarly, it is not surprising that reaction 3 exhibits the highest rate for all three mechanisms, because the secondary radical C_7H_{15}-2 or C_7H_{15}-3 forms faster than do other isomers and reaction 3 is the major consumption route of C_7H_{15}-2. Reaction 2 also consumes C_7H_{15}-2 but at a rate too slow to impact the total fuel consumption under the conditions studied. The symmetric heptyl isomer C_7H_{15}-4 is formed at a slower rate because of its lower statistical factor of only two, so that reaction 6 is of secondary importance. Reaction 6 is the slowest in the Utah mechanism and the third slowest out of five reactions in the LLNL reduced mechanism. Reaction 6 is faster than reaction 1 in the LLNL reduced mechanism, because C_7H_{15}-4 is produced at a faster rate than that of C_7H_{15}-1 in that mechanism.[18] However, the overprediction of 1-pentene in Figure 2 using the LLNL mechanism suggests that the rate of formation of C_7H_{15}-4 may be too high. Also, the β-scission rate of C_7H_{15}-4 in the LLNL mechanism, 2.65×10^8 s^{-1}, is higher than that used in the Utah mechanism, 7.94×10^7 s^{-1}, as seen in Table 1. The faster β-scission rate may also contribute to the overestimation of the 1-pentene concentration in Figure 2.

Conflicting results are obtained for reaction 5. This is because of the higher energy barrier for reactions 5 in comparison with reaction 4, as seen in Table 1, inferred by the formation of the methyl radical, which overcomes the advantage of the higher formation rate of the reactant C_7H_{15}-3. These competing effects need to be evaluated carefully. For both the Pitsch and the LLNL reduced mechanisms, the energy barrier dominates, and reaction 5 is the slowest among all β-scission reactions in these two mechanisms. The Vovelle heptane decomposition submodel[10] used in the Utah heptane mechanism probably overestimates the forward rate of reaction 5, because it yields a reaction rate at 1200 K that is even higher than that of reaction 4 (Table 1), which has the same reactant C_7H_{15}-3 but more stable products. The overestimation of the rate of reaction 5 is the major reason for the overestimation of 1-hexene by 51% using the Utah heptane mechanism, as shown in Figure 2. The enhanced rate of reaction 5 also yields a lower rate for reaction 4 so that 1-butene is underpredicted by 38% using the Utah heptane mechanism, as shown in Figure 2. In the Pitsch mechanism, reaction 5 is the major consumption route for C_7H_{15}-3, because reaction 4 is not included. The missing competing reaction route of C_7H_{15}-3 is probably the principal reason for the overprediction of 1-hexene by 30% in Figure 2 using the Pitsch mechanism.

Table 1. Arrhenius Parameters for Reactions Critically Examined

mechanism	Arrhenius parameters (mol K cm cal) A	n	E	rate at 1200 K (s^{-1})
Reaction 1. C_7H_{15}-1 = C_5H_{11}-1 + C_2H_4				
Pitsch	2.50×10^{13}	0	28824.09	1.41×10^8
Utah	2.50×10^{13}	0	28800	1.42×10^8
LLNL	8.16×10^{17}	−1.42	30840.11	8.36×10^7
Reaction 3. C_7H_{15}-2 = C_4H_9-1 + C_3H_6				
Pitsch	1.60×10^{13}	0	28322.18	1.11×10^8
Utah	1.60×10^{13}	0	28300	1.12×10^8
LLNL	2.22×10^{16}	−0.89	30130	1.31×10^8
Reaction 4. C_7H_{15}-3 = C_3H_7-1 + C_4H_8-1				
Utah	1.50×10^{13}	0	29100.48	7.51×10^7
LLNL	3.29×10^{11}	0.19	22909.89	8.50×10^7
Reaction 5. C_7H_{15}-3 = CH_3 + C_6H_{12}-1				
Pitsch	4.00×10^{13}	0	33030.59	3.85×10^7
Utah	7.94×10^{13}	0	33000	7.75×10^7
LLNL	1.027×10^{14}	−0.42	28690.01	3.11×10^7
Reaction 6. C_7H_{15}-4 = C_2H_5 + C_5H_{10}-1				
Utah	1.00×10^{13}	0	28000	7.94×10^7
LLNL	5.43×10^{16}	−0.89	30590.11	2.65×10^8
Reaction 7. C_7H_{15}-1 = C_7H_{15}-3				
Utah	2.00×10^{11}	0	11100.48	1.90×10^9
LLNL	1.386×10^9	0.98	33760	1.02×10^6
Reaction 8. C_7H_{15}-3 = C_7H_{15}-1				
Utah	3.00×10^{11}	0	14102.87	8.10×10^8
LLNL	4.41×10^7	1.38	36280	1.93×10^5
Reaction 9. C_7H_{15}-1 = C_7H_{15}-4				
Utah	2.00×10^{11}	0	18102.87	1.01×10^8
LLNL	2.541×10^9	0.35	19760	7.65×10^6
Reaction10. C_7H_{15}-4 = C_7H_{15}-1				
Utah	6.00×10^{11}	0	21102.87	8.60×10^7
LLNL	1.611×10^8	0.74	22280	2.68×10^6

Hydrogen abstraction and thermal decomposition followed by β-scission are the fundamental fuel-consumption pathways. The β-scission, which leads to one olefin and one smaller alkyl radical, is one of the first principal reactions for the decomposition of larger hydrocarbon fragments into smaller ones. Thus, an accurate description of β-scission is critical not only for the fuel consumption, but also for olefin formation, C_2−C_4 chemistry, and most likely for the whole combustion phenomena.

Concentration Buildup at Earlier Stage of Combustion. β-scission is the dominant decomposition route of alkyl radicals formed from hydrogen abstraction or thermal decomposition of the fuel. A concentration buildup process of each heptyl radical is also at work parallel to β-scission to account for some of the formation rate of alkyl radicals in the fuel consumption. It is obvious that the buildup process is important only at locations very close to the burner surface before the pseudo-steady-state of heptyl radicals is reached. For example, 39.2% of the carbon atoms released from the fuel consumption at 0.025 cm above the burner surface using the Pitsch mechanism is stored in the primary heptyl radical, not flowing into the consecutive β-scission reactions. The primary heptyl radical reaches pseudo-steady-state at 0.05 cm above the burner surface, where the formation rate of the primary heptyl radical via hydrogen abstraction is balanced by the consumption rate via β-scission. The other two mechanisms show similar patterns that buildup phenomena are observable only at very early stage of the combustion, usually less than half of a millimeter from the burner surface.

Isomerization. Isomerization reactions between alkyl radicals have very important impacts on the olefin formation chemistry. Most isomerization reactions are facilitated by a pericyclic

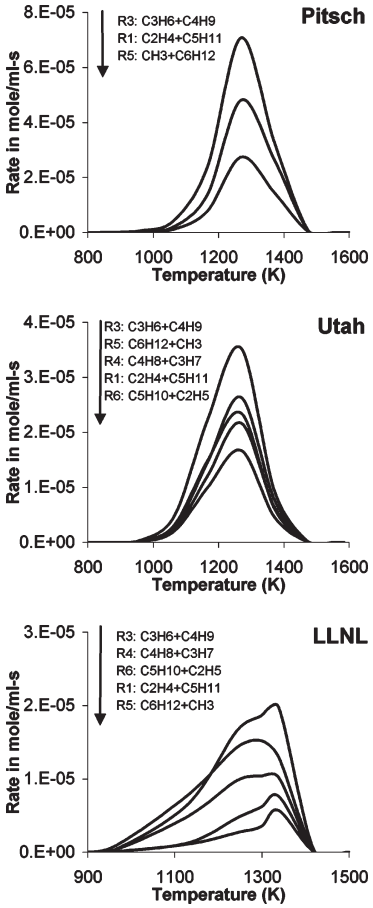

Figure 1. Relative importance of each product channel via β-scission. The arrows indicate the direction of decreasing rates. These reactions have included effects of isomerization between different heptyl radicals, which will be discussed in a later section.

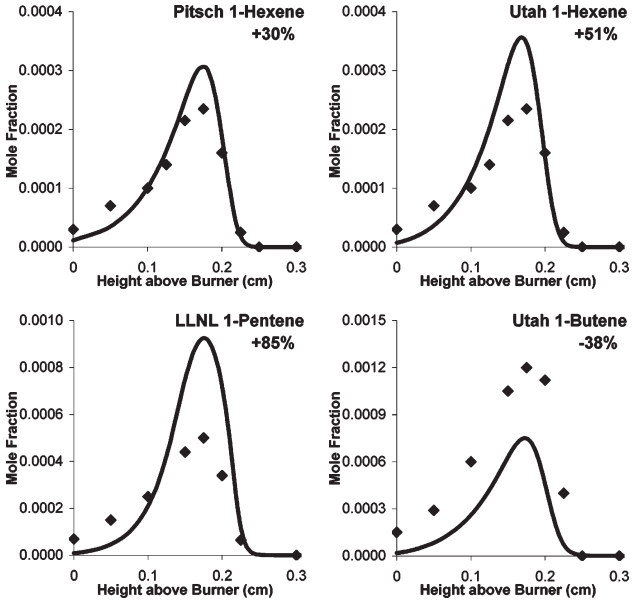

Figure 2. Comparison between simulation results and experimental data for olefins indicates uncertainties in mechanisms. Lines are for simulation results. The experimental uncertainties for these species were estimated to be lower than 20%,[2] and the numerical deviations for the simulated maximum concentrations are included for each species as a signed percentage.

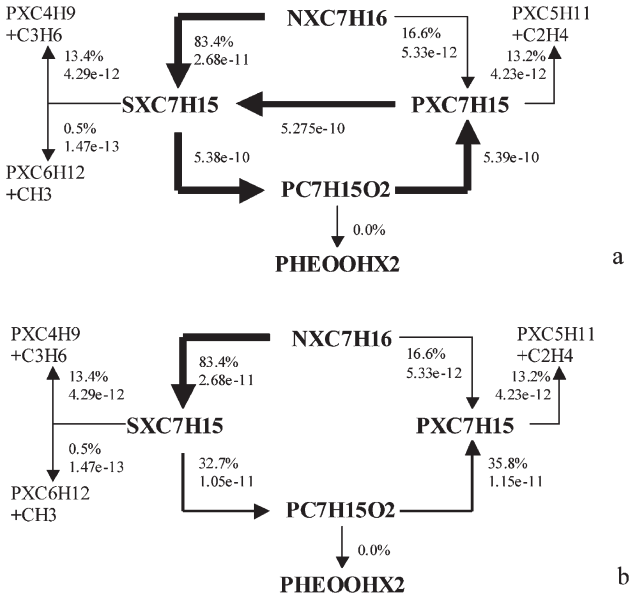

Figure 3. Indirect isomerization pathway between the primary and secondary heptyl radicals using the Pitsch mechanism at 0.025 cm (about 550 K) above the burner surface. (a) The isomerization reaction flow is bridged by the peroxy species; (b) the isomerization reaction flow bridged by the peroxy species is decycled. Reaction rate is in mol mL^{-1} s^{-1}.

reaction that forms a transient ring with five to seven members. The isomerization from C_7H_{15}-1 to C_7H_{15}-3, for example, should be the fastest reaction because it forms the most stable six-membered transition state, which is consistent with the Utah heptane mechanism.

Isomerization Reactions in the Pitsch Mechanism. Because the Pitsch mechanism does not distinguish between secondary heptyl radical isomers, there is only one isomerization reaction between the primary and the lumped secondary radicals in addition to an indirect isomerization route bridged by the peroxy radicals. For instance, at 0.025 cm above the burner surface (550 K), as indicated in Figure 3a, there is a cycle from the primary heptyl radical (PXC_7H_{15}) to the secondary heptyl radical (SXC_7H_{15}) via hydrogen migration, to heptyl peroxy radical ($PC_7H_{15}O_2$) via molecular oxygen addition, and back to the primary heptyl radical by breaking the C−O bond. It is noted, however, that the $PC_7H_{15}O_2$ radical is a lumped species without specifying the substitution site in the Pitsch mechanism, and starts the low-temperature chemistry by forming a diperoxy heptyl radical after an internal hydrogen migration, resulting in the formation of a hydroperoxy alkyl radical ($PHEOOHX_2$ in Figure 3).

The rate of each reaction and its share of the total fuel consumption rate are shown along the arrow indicating the reaction direction. At low temperatures (<1000 K), thermal decomposition consumes only a trivial portion of the fuel, and a majority of the carbon atoms in the fuel are converted into heptyl radicals. Because the isomerization reactions are faster than the decomposition reactions, a heptyl radical may change its structure many times between the two isomers before a β-scission reaction can happen. The result is a much larger flow inside the isomerization cycle than the carbon flow that is actually released from the fuel decomposition. For example, the isomerization rate between the two heptyl isomers is about 20 times larger than the net hydrogen-abstraction rate, as shown in Figure 3a. The isomerization via the peroxy radical might be greatly slowed down, however, by adding a conversion reaction between the primary and the secondary peroxy radicals, which are not distinguished in the Pitsch Mechanism

secondary heptyl ⇔ secondary peroxy ⇔
primary peroxy ⇔ primary heptyl

Otherwise, a black box approach is useful here by treating the cycle as a single unit for which only carbon atom inflow and outflow are considered in order to find the direction of the net isomerization reaction between the two heptyl isomers. This method of representation is shown in Figure 3b, and the isomerization reaction rate in the direction from the secondary toward the primary radical accounts for 30−35% of the net fuel consumption rate. The concentration ratio of the secondary over the primary radical is at least three to one if the temperature is lower than 1000 K. Thus the abundance of the secondary heptyl radical is the dominant factor in establishing the rates of isomerization in the Pitsch mechanism at low temperatures. The isomerization reaction via peroxy radical becomes trivial and the relative rates of isomerization pathways reverse at higher temperatures because the formation rate of the primary radical gradually catches up to that of the secondary radical. The relative formation rate of each heptyl radical becomes of secondary importance to the lower activation energy of isomerization reactions. The rate of isomerization from the primary to the secondary radical is favored by the lower energy barrier, because the primary radical has higher energy than its secondary isomer. As a consequence, at temperatures higher than 1000 K, the secondary radical is produced from the primary radical because of equilibrium considerations.

Isomerization Reactions in the LLNL and the Utah Mechanisms. The LLNL and Utah heptane mechanisms feature four isomerization reactions between the heptyl radicals. Because C_7H_{15}-2 and C_7H_{15}-3 radicals are formed at almost the same rates by hydrogen abstraction, the isomerization direction between C_7H_{15}-2 and C_7H_{15}-3 depends heavily on other isomerization and β-scission reactions that will change the concentrations of these two chemically similar radicals. Both the LLNL and the Utah heptane mechanisms exhibit some direction switching for the isomerization reaction between C_7H_{15}-2 and C_7H_{15}-3. Although the isomerization reactions between the primary and secondary heptyl radicals always favor the secondary radical, there are two exceptions. At very low temperatures, the combustion chemistry may favor the abundance of reactant over the lower energy barrier. This reversion of the isomerization reaction direction is obvious in the Pitsch mechanism via the peroxy cycle, but is barely observable at only very low temperatures (<650 K) for the isomerization reaction between C_7H_{15}-1 and C_7H_{15}-2 in the Utah heptane mechanism. The second exception comes from the isomerization of C_7H_{15}-1 and its symmetric isomer C_7H_{15}-4. The rate of the isomerization from C_7H_{15}-4 to C_7H_{15}-1 is favored by the statistical factor, because six hydrogen atoms at both ends of the molecule can migrate compared to two of them for the reverse reaction. On the other hand, the direction from C_7H_{15}-1 to C_7H_{15}-4 is preferred because of the lower energy barrier, as discussed earlier. The higher statistical factor competes with the lower energy barrier in determining the net isomerization direction. In the LLNL-reduced mechanism, the effects of the lower energy barrier (by 10 kJ) are more important, whereas in the Utah mechanism, the higher statistical factor (by a factor of 3) is more significant, as seen in Table 1 for reactions 9 and 10. Opposite directions are assigned to this isomerization reaction by the LLNL and the Utah heptane mechanisms that may have a significant influence on the concentration profiles of some larger olefins. As shown in Figure 4, the formation rate of C_7H_{15}-4 decreases by as much as 25% in the Utah mechanism compared to a modest 5% gain for the C_7H_{15}-4 formation in the LLNL model. This reduction of C_7H_{15}-4 formation may account for the better prediction (7% deviation) of 1-pentene obtained using the Utah heptane mechanism. The preferential formation by isomerization, a too high formation rate by hydrogen abstraction,[18] and a too fast decomposition of C_7H_{15}-4 (as discussed earlier in the β-scission section) may all contribute to the 85% overprediction of 1-pentene (Figure 2) using the LLNL mechanism.

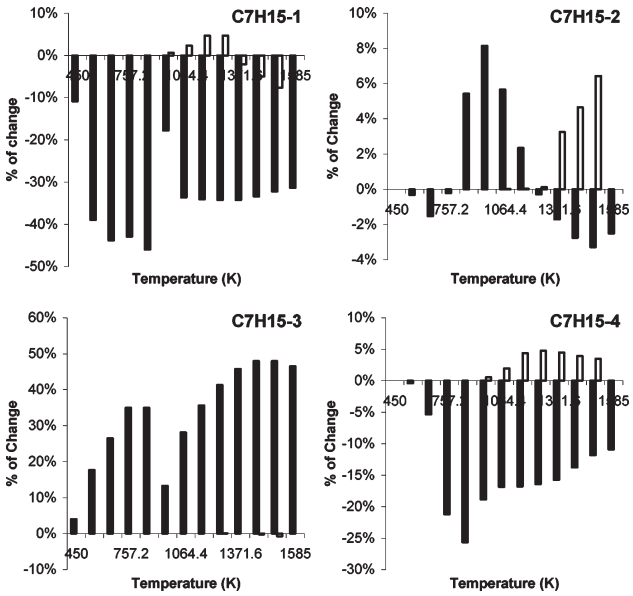

Figure 4. Percentage change of heptyl radical formation rate when isomerization reactions are included. Black bars are for the Utah heptane mechanism; white bars are for the LLNL reduced mechanism.

C_7H_{15}-3 radical is another heptyl isomer of importance. In the LLNL mechanism, both directions of the isomerization reaction between C_7H_{15}-1 and C_7H_{15}-3 are one order of magnitude slower than the corresponding reactions between C_7H_{15}-1 and C_7H_{15}-4. In contrast, the isomerization reactions between C_7H_{15}-1 and C_7H_{15}-3 in the Utah mechanism are one order of magnitude faster than those between C_7H_{15}-1 and C_7H_{15}-4, which indicates a preference in the Utah mechanism for a transition state of a six-membered ring. The LLNL mechanism shows almost no obvious isomerization effects, whereas the Utah mechanism suggests an increase in C_7H_{15}-3 formation by as much as 50%. This preferential formation via isomerization, as well as the acceleration of the β-scission rate as discussed earlier, may contribute to the overestimation of 1-hexene by 51% using the Utah heptane mechanism as shown in Figure 2. The majority of the increase in C_7H_{15}-3 is at the expense of C_7H_{15}-1, the formation rate of which is slowed down by 30−40%. However, the impacts of this reduction are hardly visible when compared to experimental data, because the decomposition of C_7H_{15}-1 to $C_2H_4 + C_5H_{11}$-1 is not the major formation route for ethylene.

In general, the Utah heptane mechanism involves some very active isomerization reactions. As shown in Figure 4, the change in heptyl isomer formation rates due to isomerization is at least a factor of five larger using the Utah mechanism than that obtained using the LLNL mechanism except for the least active isomer, C_7H_{15}-2.

Evolution of Olefins. Among the three mechanisms, the Pitsch mechanism provides the smallest olefin reaction set, namely 1-hexene, 1-butene, propylene, and ethylene. Both the LLNL and the Utah heptane mechanisms give a full set of olefin species from C_2 to C_7, including all three heptene isomers. The

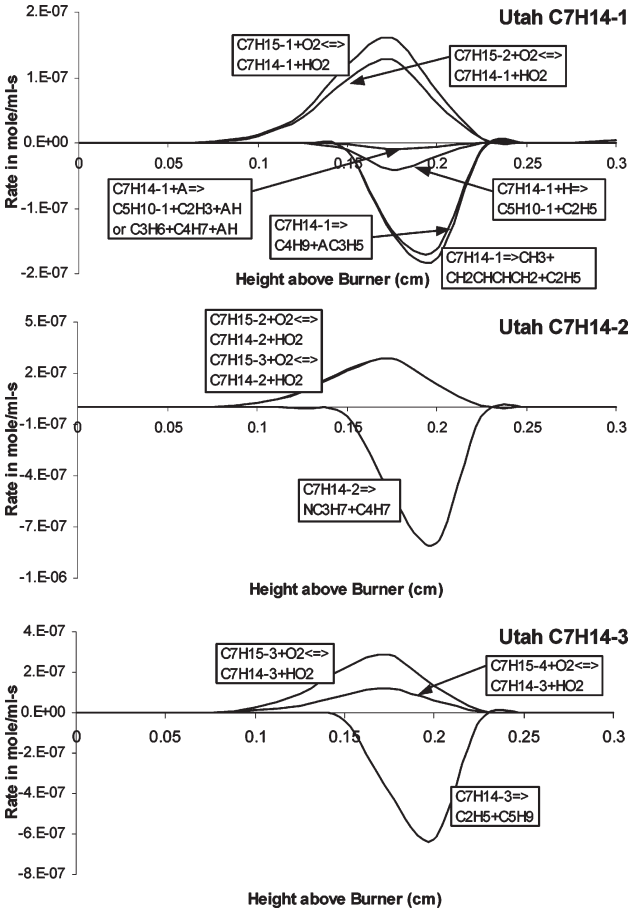

Figure 5. Formation and consumption reactions of heptene isomers using the Utah mechanism.

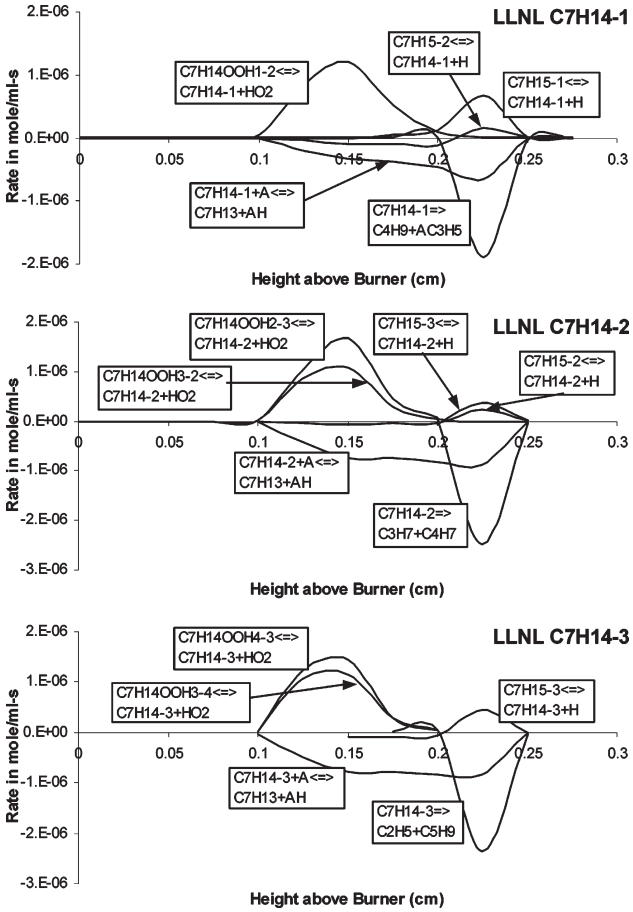

Figure 6. Formation and consumption reactions of heptene isomers using the LLNL mechanism.

Utah heptane mechanism has the most complete set that also includes all three butene isomers, 1-butene, 2-butene, and isobutylene. Major olefin formation and consumption reactions in the *n*-heptane premixed flame are listed in Table 2, as well as the maximum rates of these reactions and the temperatures at which the maximum rates are reached.

Formation and Consumption of Heptene Isomers. Olefin chemistry is very different from model to model, as illustrated in Figures 5 and 6 for the formation and consumption of heptene isomers using the LLNL and Utah heptane mechanisms. The most important pathway to heptene formation provided by the Utah heptane mechanism for all three isomers is hydrogen abstraction by O_2.

$$C_7H_{15}\text{-}1 + O_2 \leftrightarrow C_7H_{14}\text{-}1 + HO_2$$

$$C_7H_{15}\text{-}2 + O_2 \leftrightarrow C_7H_{14}\text{-}1 + HO_2$$

$$C_7H_{15}\text{-}2 + O_2 \leftrightarrow C_7H_{14}\text{-}2 + HO_2$$

$$C_7H_{15}\text{-}3 + O_2 \leftrightarrow C_7H_{14}\text{-}2 + HO_2$$

$$C_7H_{15}\text{-}3 + O_2 \leftrightarrow C_7H_{14}\text{-}3 + HO_2$$

$$C_7H_{15}\text{-}4 + O_2 \leftrightarrow C_7H_{14}\text{-}3 + HO_2$$

These reactions become important at 850 K and reach their maximum rates around 1170 K. Near 1400 K, these reactions become trivial.

The Utah heptane mechanism includes three major consumption routes of heptene isomers. Each heptene isomer can be consumed by thermal decomposition into alkyl and allylic radicals (reactions D[17], D[19], and D[22] in Table 2). The bond broken is usually the C−C σ bond between the α and β carbons, because allylic radicals are the most stable of the possible products. Also of importance is the formation of 1,3-butadiene from 1-heptene decomposition (D[16]), which is the most active consumption route for that heptene isomer. This pathway, however, is not promoted in the Pitsch and LLNL mechanisms. Therefore, an examination of the kinetics of 1-heptene decomposition is necessary and will be presented in a future publication. Hydrogen addition followed by β-scission is a fast chemically activated reaction and represents the third most active consumption pathway of 1-heptene, but this reaction class is not involved for other heptene isomers. In a future publication, this reaction class will be incorporated into the Utah mechanism for other olefins in order to lower numerical deviations of these species. Hydrogen abstraction followed by β-scission (HA[20] and HA[23]) is a minor consumption route for all three heptene isomers. Depending on the abstraction site, the alkenyl radical intermediate can break into C_2-C_5 olefins plus one smaller alkenyl radical. All consumption reactions start around 1000 K and reach their maximum rates at 1270 K. The mechanism does not include reactions involving the formation of diene species via hydrogen abstraction of large olefins, and these reactions should be examined in future mechanism improvements.

Because the LLNL mechanism includes low-temperature chemistry that involves peroxy radicals, its olefin formation has many unique features, as shown in Figure 6. There are two classes of major formation reactions. For temperatures lower than 900 K, heptene isomers are formed exclusively from the

Table 2. Formation and Consumption Reactions of Olefin Species

	formation reactions						consumption reactions					
species	type[a]	T_{max}	max rate[b]	type[a]	T_{max}	max rate[b]	type[a]	T_{max}	max rate[b]	type[a]	T_{max}	max rate[b]
						Pitsch Mechanism						
C_6H_{12}	D^{1}	1269	2.74×10^{-5}				D^{2}	1269	2.54×10^{-5}	HA^{3}	1269	1.83×10^{-6}
C_4H_8	C^{4}	1269	2.19×10^{-5}				D^{5}	1372	2.76×10^{-5}	AD^{6}	1372	2.18×10^{-6}
C_3H_6	D^{7}	1269	7.08×10^{-5}	C^{8}	1372	1.82×10^{-5}	A^{9}	1372	5.70×10^{-5}	HA^{10}	1372	2.87×10^{-5}
C_2H_4	D^{11}	1371	1.15×10^{-4}	D^{12}	1269	8.61×10^{-5}	HA^{13}	1372	4.15×10^{-4}	D^{14}	1474	1.81×10^{-7}
						Utah Mechanism						
C_7H_{14}-1	HA^{15}	1167	2.88×10^{-7}				D^{16}	1269	1.78×10^{-7}	D^{17}	1269	1.62×10^{-7}
C_7H_{14}-2	HA^{18}	1167	5.68×10^{-7}				D^{19}	1269	7.95×10^{-7}	HA^{20}	1167	7.39×10^{-8}
C_7H_{14}-3	HA^{21}	1167	4.04×10^{-7}				D^{22}	1269	6.09×10^{-7}	HA^{23}	1167	7.63×10^{-9}
C_6H_{12}	D^{24}	1269	2.64×10^{-5}				D^{25}	1269	2.08×10^{-5}	HA^{26}	1269	5.72×10^{-6}
C_5H_{10}	D^{27}	1269	1.67×10^{-5}				D^{28}	1372	5.58×10^{-6}	AD^{29}	1269	6.90×10^{-6}
C_4H_8	D^{30}	1269	2.35×10^{-5}	D^{31}	1269	3.86×10^{-6}	HA^{32}	1269	1.34×10^{-5}	AD^{33}	1269	1.63×10^{-5}
C_3H_6	A^{34}	1372	4.43×10^{-5}	D^{35}	1269	3.53×10^{-5}	HA^{36}	1372	5.70×10^{-5}	AD^{37}	1372	4.20×10^{-5}
C_2H_4	D^{38}	1269	1.10×10^{-4}	D^{39}	1269	9.10×10^{-5}	HA^{40}	1474	1.86×10^{-4}	AD^{41}	1474	7.35×10^{-5}
						LLNL Reduced Mechanism						
C_7H_{14}-1	D^{42}	811	1.21×10^{-6}	D^{43}	1338	8.41×10^{-7}	D^{44}	1338	1.90×10^{-6}	HA^{45}	1338	6.63×10^{-7}
C_7H_{14}-2	D^{46}	811	2.74×10^{-6}	D^{47}	1338	6.01×10^{-7}	D^{48}	1338	2.49×10^{-6}	HA^{49}	1338	8.69×10^{-7}
C_7H_{14}-3	D^{50}	811	2.60×10^{-6}	D^{51}	1338	4.73×10^{-7}	D^{52}	1338	2.36×10^{-6}	HA^{53}	965	8.30×10^{-7}
C_6H_{12}	D^{54}	1338	5.63×10^{-6}	HA^{55}	1338	6.81×10^{-7}	D^{56}	1338	1.09×10^{-5}	HA^{57}	1338	3.69×10^{-6}
C_5H_{10}	D^{58}	965	1.04×10^{-5}	C^{59}	965	2.62×10^{-6}	D^{60}	1338	2.05×10^{-5}	A^{61}	1338	5.13×10^{-6}
C_4H_8	D^{62}	965	1.52×10^{-5}	A^{63}	1338	3.44×10^{-6}	HA^{64}	1338	2.37×10^{-5}	D^{65}	1338	7.80×10^{-6}
C_3H_6	D^{66}	1338	1.03×10^{-4}	A^{67}	1338	6.27×10^{-5}	HA^{68}	1338	1.04×10^{-4}	NC^{69}	1338	9.03×10^{-5}
C_2H_4	D^{70}	1338	1.46×10^{-4}	D^{71}	1338	8.75×10^{-5}	HA^{72}	1499	1.66×10^{-4}			

Reactions Corresponding to Numbers in Types Listed Above

1. $SXC_7H_{15} \rightarrow PXC_6H_{12} + CH_3$;
2. $PXC_6H_{12} \rightarrow NXC_3H_7 + C_3H_5$;
3. $PXC_6H_{12} + A \rightarrow C_6H_{11} + AH$;
4. $C_3H_5 + CH_3 \leftrightarrow PXC_4H_8$;
5. $PXC_4H_8 \leftrightarrow C_3H_5 + CH_3$;
6. $PXC_4H_8 + OH \leftrightarrow NXC_3H_7 + CH_2O$;
7. $SXC_7H_{15} \rightarrow PXC_4H_9 + C_3H_6$;
8. $C_2H_3 + CH_3 \leftrightarrow C_3H_6$;
9. $C_3H_6 + H \leftrightarrow NXC_3H_7$;
10. $C_3H_6 + A \leftrightarrow C_3H_5 + AH$;
11. $NXC_3H_7 \leftrightarrow CH_3 + C_2H_4$;
12. C_2H_5 (+M) $\leftrightarrow C_2H_4 + H$ (+M);
13. $C_2H_4 + H \leftrightarrow C_2H_3 + H_2$;
14. C_2H_4 (+M) $\leftrightarrow C_2H_2 + H_2$ + M;
15. C_7H_{15}-1(2) + $O_2 \leftrightarrow C_7H_{14}$-1 + HO_2;
16. C_7H_{14}-1 $\rightarrow CH_3 + C_4H_6$-13 + C_2H_5;
17. C_7H_{14}-1 $\rightarrow C_4H_9$-1 + AC_3H_5;
18. C_7H_{15}-2(3) + $O_2 \leftrightarrow C_7H_{14}$-2 + HO_2;
19. C_7H_{14}-2 $\rightarrow NC_3H_7 + NC_4H_7$;
20. C_7H_{14}-2 + A $\rightarrow$ products + AH;
21. C_7H_{15}-3(4) + $O_2 \leftrightarrow C_7H_{14}$-3 + HO_2;
22. C_7H_{14}-3 $\rightarrow C_2H_5 + C_5H_9$;
23. C_7H_{14}-3 + A $\rightarrow$ products + AH;
24. C_7H_{15}-3 $\leftrightarrow C_6H_{12}$-1 + CH_3;
25. C_6H_{12}-1 $\rightarrow NC_3H_7 + AC_3H_5$;
26. C_6H_{12}-1 + A $\leftrightarrow$ products + AH;
27. C_7H_{15}-4 $\leftrightarrow C_5H_{10}$-1 + C_2H_5;
28. C_5H_{10}-1 $\rightarrow AC_3H_5 + C_2H_5$;
29. C_5H_{10}-1 + H $\leftrightarrow$ products;
30. C_7H_{15}-3 $\leftrightarrow C_4H_8$-1 + NC_3H_7;
31. C_6H_{11}-1 $\leftrightarrow C_4H_8$-1 + C_2H_3;
32. C_4H_8-1 + H $\leftrightarrow$ products + AH;
33. C_4H_8-1 + A $\leftrightarrow$ products;
34. $AC_3H_5 + H \leftrightarrow C_3H_6$;
35. C_7H_{15}-2 $\leftrightarrow C_3H_6 + C_4H_9$-1;
36. C_3H_6 + A $\leftrightarrow$ products + AH;
37. C_3H_6 + A $\leftrightarrow$ products;
38. C_2H_5 (+M) $\leftrightarrow C_2H_4 + H$ (+M);
39. $NC_3H_7 \leftrightarrow CH_3 + C_2H_4$;
40. $C_2H_4 + A \leftrightarrow C_2H_3 + AH$;
41. $C_2H_4 + A$ = products;
42. $C_7H_{14}OOH1$-2 $\leftrightarrow C_7H_{14}$-1 + HO_2;
43. C_7H_{15}-1(2) $\leftrightarrow C_7H_{14}$-1 + H;
44. C_7H_{14}-1 $\leftrightarrow PC_4H_9 + C_3H_5$-A;
45. C_7H_{14}-1 + A $\rightarrow C_7H_{13}$ + AH;
46. $C_7H_{14}OOH2-3(3-2) \leftrightarrow C_7H_{14}$-2 + HO_2;
47. C_7H_{15}-2(3) $\leftrightarrow C_7H_{14}$-2 + H;
48. C_7H_{14}-2 $\leftrightarrow NC_3H_7 + C_4H_7$;
49. C_7H_{14}-2 + A $\rightarrow C_7H_{13}$ + AH;
50. $C_7H_{14}OOH3-4(4-3) \leftrightarrow C_7H_{14}$-3+$HO_2$;
51. C_7H_{15}-3(4) $\leftrightarrow C_7H_{14}$-3 + H;
52. C_7H_{14}-3 $\leftrightarrow NC_3H_7 + C_4H_7$;
53. C_7H_{14}-3 + A $\rightarrow C_7H_{13}$ + AH;
54. C_7H_{15}-3 $\leftrightarrow C_6H_{12}$-1 + CH_3;
55. $C_7H_{14}O1-3$ + OH $\leftrightarrow C_6H_{12}$-1 + HCO + H_2O;
56. C_6H_{12}-1 $\leftrightarrow NC_3H_7 + C_3H_5$-A;
57. C_6H_{12}-1 + A $\rightarrow C_6H_{11}$ + AH;
58. C_7H_{15}-4 $\leftrightarrow C_5H_{10}$-1 + C_2H_5;
59. $C_2H_5 + C_3H_5$-A $\leftrightarrow C_5H_{10}$-1;
60. C_5H_{10}-1 $\leftrightarrow C_2H_5 + C_3H_5$-A;
61. C_5H_{10}-1 + H $\leftrightarrow C_5H_{11}$-X;
62. C_7H_{15}-3 $\leftrightarrow C_4H_8$-1 + NC_3H_7;
63. $C_4H_7 + H \leftrightarrow C_4H_8$-1;
64. C_4H_8-1 + A $\rightarrow C_4H_7$ + AH;
65. C_4H_8-1 $\leftrightarrow C_3H_5$-A + CH_3;
66. $IC_3H_7 \leftrightarrow C_3H_6 + H$;
67. C_3H_5-A + H $\leftrightarrow C_3H_6$;
68. C_3H_6 + A $\leftrightarrow$ products + AH;
69. $C_3H_6 + H_2 \leftrightarrow IC_3H_7 + H$;
70. C_2H_5 (+M) $\leftrightarrow C_2H_4 + H$ (+M);
71. $NC_3H_7 \leftrightarrow C_2H_4 + CH_3$;
72. $C_2H_4 + H \leftrightarrow C_2H_3 + H_2$;

[a] Code for type: D = decomposition, A = addition, C = combination, NC = not classified, HA = hydrogen abstraction, AD = addition and then decomposition. [b] Maximum rate in units of mol cm^{-3} s^{-1} and K.

decomposition of α-hydroperoxy heptyl radicals. For example, C_7H_{14}-2 is formed via the reaction of

$$CH_3-CH(OOH)-CH^{\bullet}-CH_2-CH_2-CH_2-CH_3 = C_7H_{14}\text{-}2 + HO_2$$

When the flame temperature reaches 1000 K, dehydrogenation reactions of heptyl radicals exceed low-temperature peroxy radical reactions for the formation of heptene isomers. Although the heptene formation is very different in the LLNL and Utah heptane mechanisms, both mechanisms share a few common consumption reactions. For the LLNL mechanism, thermal decomposition is also identified to be the major consumption pathway of heptene isomers. These reactions (D^{44}, D^{48}, and D^{52}) start around 1000 K and reach their maximum rates at 1350 K. Hydrogen abstraction is also recognized as the competing consumption route and makes greater contributions to the net consumption rates of heptene isomers than corresponding reactions in the Utah heptane mechanism. These reactions (HA^{45}, HA^{49}, and HA^{53}) start early in the low-temperature region and offer an outlet for heptene isomers that are formed from the decomposition of α-hydroperoxy heptyl radicals. Hydrogen-abstraction reactions reach their maximum rates, however, in the high-temperature region, where thermal decomposition reactions are also most active.

Formation and Consumption of Other Olefins. Despite the model-dependent differences in reactions of heptene isomers, the chemistry of other olefins is very similar for all three mechanisms, especially for larger olefins. Reactions that involve oxygenated compounds of low-temperature chemistry show some importance for the formation of 1-hexene in the LLNL mechanism (HA^{55}) but with a rate that is one order of magnitude lower than that of the competing β-scission reaction (D^{54}). Besides 1-hexene, those reactions that involve oxygenates are

Table 3. Possible Reasons of Differences between Simulated and Experimental Results

species	model	deviation	reaction class	possible reasons
C_7H_{14}-1	LLNL	×10	low T	
C_7H_{14}-2	LLNL	×12	low T	The importance of α-hydroperoxy radical decomposition is probably overstated.
C_7H_{14}-3	LLNL	×19	low T	
C_7H_{14}-2	Utah	+100%	H addition	Missing hydrogen addition followed by β-scission reactions for 2-heptene
C_7H_{14}-3	Utah	+125%	H addition	and 3-heptene consumption.
C_6H_{12}-1	Pitsch	30%	β-scission	There are not enough competing routes for secondary heptyl radical β-scission. For example, no SXC_7H_{15} => $NC_3H_7 + C_4H_8$-1. Thus, the reaction toward C_6H_{12}-1 is overfed.
C_6H_{12}-1	Utah	51%	β-scission	The decomposition 3-heptyl radical toward $CH_3 + C_6H_{12}$-1 should be less active
C_4H_8-1	Utah	−38%	β-scission	than the one toward $NC_3H_7 + C_4H_8$-1 because the activation energy of the first reaction is higher.
C_6H_{12}-1	Utah	51%	isomerization	C7H15-3 formation gains 50% from isomerization.
C_5H_{10}-1	LLNL	85%	H abstraction	The formation rate of symmetric 4-heptyl radical is probably overestimated.
C_5H_{10}-1	LLNL	85%	isomerization	C7H15-4 formation gains from C7H15-1 isomerization.
C_5H_{10}-1	LLNL	85%	β-scission	The rate may be too fast coupled with hydrogen abstraction and isomerization gains.

of secondary importance for the formation of other olefins. The β-scission is almost the exclusive formation route of 1-hexene for all three mechanisms (D^1, D^{24}, and D^{54}), and also dominates the formation of 1-pentene using the LLNL (D^{58}) and the Utah heptane mechanisms (D^{27}). The LLNL model also yields a smaller rate of formation of 1-pentene from the combination of ethyl and allyl radicals (C^{59}), corresponding to about 20% of the total.

There are some disagreements between mechanisms for the chemistry of 1-butene. Combination of the allyl and methyl radicals is the exclusive formation route in the Pitsch mechanism (C^4), whereas in the Utah mechanism, 1-butene formation results from two β-scission reactions of 3-heptyl radical (D^{30}, major formation route) and hexyl radical (D^{31}, minor formation route). The LLNL mechanism includes the β-scission of the 3-heptyl radical (D^{62}, major formation route) in addition to the hydrogenation of butenyl radical (A^{63}, minor formation route).

There are also differences in approaches to propylene formation. The Pitsch mechanism includes a β-scission of the secondary heptyl radical (D^7, major formation route) and the combination of methyl and vinyl radicals (C^8, minor formation route). In the Utah heptane mechanism, the β-scission of the 2-heptyl radical (D^{35}) is the second most important formation route that is exceeded only by the slightly faster hydrogenation of 3-propenyl (or allyl) radical (A^{34}). The importance of allyl radical hydrogenation is also recognized in the LLNL mechanism (A^{67}), but the reaction is 30% slower than the competing formation pathway via the dehydrogenation of 2-propyl radical (D^{66}). There are growing differences in the major formation reactions as the size of olefin is reduced. There is, however, general agreement on the mechanism of ethylene formation. Ethylene is formed either by the decomposition of 1-propyl radical (D^{11}, D^{39}, and D^{71}) or by the dehydrogenation of ethyl radical (D^{12}, D^{38}, and D^{70}), and both pathways have almost equal importance.

Although the olefin formation chemistry differs between mechanisms, the consumption of olefin is limited to a few reaction classes, with frequent agreement between the three mechanisms. For example, the consumption of 1-hexene for all three mechanisms is mostly by the thermal decomposition into 1-propyl and allyl radicals (D^2, D^{25}, and D^{56}), augmented by a minor route through hydrogen abstraction (HA^3, HA^{26}, and HA^{57}). Thermal decomposition and hydrogen addition are the major consumption routes of 1-pentene for both the LLNL (D^{60} and A^{61}) and the Utah (D^{28} and AD^{29}) heptane mechanisms. Three consumption reaction classes are assigned to 1-butene. The Pitsch mechanism considers the thermal decomposition reaction that forms methyl and allyl radicals (D^5, major route) in addition to a minor addition followed by decomposition reaction (AD^6). Hydrogen abstraction is considered to be the most important consumption pathway in the other two mechanisms (HA^{32} and HA^{64}). The second outlet for 1-butene, in the Utah mechanism, is the addition and decomposition reaction (AD^{33}), and in the LLNL model is the thermal decomposition reaction (D^{65}). Hydrogen abstraction (HA^{10}, HA^{36}, and HA^{68}) and addition (A^9, AD^{37}, and NC^{69}) qualify, almost equally, as the major consumption pathways of propylene for all three mechanisms. Hydrogen abstraction is also the exclusive consumption route for ethylene using the Pitsch (HA^{13}) and LLNL (HA^{72}) mechanisms and the principal pathway using the Utah mechanism (HA^{40}), which also includes a competing route of hydrogen addition followed by decomposition reaction (AD^{41}), corresponding to about 30% of the total consumption rate.

Discussion

Summary of Findings. Olefin chemistry is the major focus of this study because it is a fundamental building block in the generation of combustion mechanisms for larger paraffins. Olefin formation relies heavily on the β-scission of alkyl radicals except for the conjugate or the smallest olefins. β-scission, which leads to one olefin and one smaller alkyl radical, is the principal pathway in the cracking of larger hydrocarbon fragments. In a normal heptane premixed flame, heptene formation occurs mainly via hydrogen abstraction by O_2 in the Utah mechanism or via decomposition of α-hydroperoxy heptyl radicals in the LLNL mechanism. Formation of smaller olefins also occurs via hydrogen addition and combination reactions (e.g., reactions C^8, A^{34}, A^{63}, A^{67}; see Table 2). Larger olefins are consumed mainly by thermal decomposition and sometimes by a minor route of hydrogen abstraction followed by decomposition. Hydrogen abstraction is primarily responsible for the decomposition of smaller olefins. In some occasions, the addition of a radical onto an olefin followed by decomposition also consumes a portion of the olefin reactant. Isomerization between heptyl radicals also influences the formation of olefins because isomerization may change the formation rates of heptyl radicals by as much as 50%, as shown in Figure 4.

Major reaction pathways of olefin species that are identified in this work will aid the mechanism generation efforts, as well as those of mechanism reduction. Resulting mechanisms with a manageable size that include these important reaction classes are crucial for fast and reliable numerical solutions that can satisfy a number of simulation goals.

Areas of Uncertainty in Olefin Chemistry. The extension of major reaction classes in normal heptane flames to larger

paraffins can be done only if the numerical accuracy of the base model lives up to the expectations of simulation requirements. When the numerical performance is not quite satisfactory or even misleading, the base model needs to be corrected before it can be extended. Reaction pathway analysis has been found to be a good tool for improving the numerical performance of an existing mechanism. There are a number of illustrations in this work where possible reasons for numerical deviations are identified by use of reaction pathway analysis. For example, the overestimation of the peak concentration of 1-hexene by 51% using the Utah heptane mechanism is probably due to the combined effects of a faster β-scission of C_7H_{15}-3 and a preferential formation of C_7H_{15}-3 via isomerization of heptyl radicals. Areas of uncertainty for selected olefin species are summarized in Table 3. Understanding of olefin chemistry is key to the modeling of paraffin consumption because olefins are the most direct products from fuel decomposition. Numerical deviation of other species as well as some smallest olefins such as ethylene and propylene involves more reactions and is thus more difficult to diagnose.

The principal goal of this study is to identify major formation and consumption pathways of olefins as well as areas of uncertainty of these reactions in three different heptane mechanisms rather than that of promoting any particular mechanism. It is also important to know that the Vovelle heptane submechanism[10] was chosen in the Utah mechanism to simulate a premixed flame measured by the same French group. Thus the generally good agreement of the Utah heptane mechanism with the experimental data of this heptane flame may not guarantee the same performance for other experimental results. The ability of any of the three mechanisms to fit experimental data is expected to vary from experiment to experiment.

It is noteworthy that the models analyzed in this work were not developed originally for olefin chemistry. Therefore, each model inevitably has some weakness and incompleteness in predicting olefin yields. Resolution of the sources of differences between the mechanisms identified above would contribute to the development of a more robust model applicable to all systems. An improved mechanism that targets the combustion of normal heptane and other higher paraffins will be developed and its numerical performance will be presented in a future study.

Acknowledgment. This research was funded by the University of Utah (C-SAFE), through a contract with the Department of Energy, Lawrence Livermore National Laboratory (B341493). The authors thank Dr. Charlie Westbrook and Dr. Bill Pitz for helpful discussions and general guidance in combustion modeling of practical fuels and Professor Christian Vovelle for his help in interpretation of experimental data.

EF060195H